Ecotoxicology and Environmental Safety 269 (2024) 115752

Contents lists available at ScienceDirect

Ecotoxicology and Environmental Safety

journal homepage: www.elsevier.com/locate/ecoenv

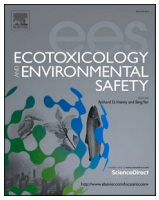

Integrative transcriptome and metabolome analysis of fluoride exposure induced developmental neurotoxicity in mouse brain

Xinliang Zhu [a,c,d,*], Shunbin Zhang [a], Xiaoxiao Liu [f], Huixia Li [g], Xinyu Zhu [e], Ji Zhang [a,c,d], Xiaopeng Wang [e], Min Zhang [b,e,**]

[a] College of Life Science, Northwest Normal University, Lanzhou 730070, Gansu Province, China
[b] Department of Scientific Research, Gansu Provincial Hospital, Lanzhou 730000, China
[c] Bioactive Products Engineering Research Center for Gansu Distinctive Plants, Lanzhou 730070, China
[d] Institute of Rural Development and Research, Northwest Normal University, Lanzhou 730070, Gansu Province, China
[e] Department of General Surgery, Gansu Provincial Hospital, Lanzhou 730000, China
[f] Lanzhou Institute of Food and Drug Control, Lanzhou 740050, China
[g] Gansu Tongxing Intelligent Technology Development Co., Ltd., Lanzhou 730070, Gansu Province, China

ARTICLE INFO

Edited by Mohamed Abdel-Daim

Keywords:
Fluoride
Transcriptomics
Metabolomics
Developmental neurotoxicity
Choline metabolism
Arachidonic acid metabolism

ABSTRACT

Fluoride could cause developmental neurotoxicity and significantly affect the intelligence quotient (IQ) of children. However, the systematic mechanism of neuronal damage caused by excessive fluoride administration in offspring is largely unknown. Here, we present a comprehensive integrative transcriptome and metabolome analysis to study the mechanism of developmental neurotoxicity caused by chronic fluoride exposure. Comparing the different doses of fluoride treatments in two generations revealed the exclusive signature of metabolism pathways and gene expression profiles. In particular, neuronal development and synaptic ion transport are significantly altered at the gene expression and metabolite accumulation levels for both generations, which could act as messengers and enhancers of fluoride-induced systemic neuronal injury. Choline and arachidonic acid metabolism, which highlighted in the integrative analysis, exhibited different regulatory patterns between the two generations, particularly for synaptic vesicle formation and inflammatory factor transport. It may suggest that choline and arachidonic acid metabolism play important roles in developmental neurotoxic responses for offspring mice. Our study provides comprehensive insights into the metabolomic and transcriptomic regulation of fluoride stress responses in the mechanistic explanation of fluoride-induced developmental neurotoxicity.

1. Introduction

Fluoride is considered an essential trace element for humans and animals to prevent dental caries, but it can also cause dental fluorosis if too much fluoride is ingested during tooth development. Since fluoride can diffuse into drinking water and the environment, excessive fluoride intake can harm various organs, such as the occurrence of skeletal fluorosis (Srivastava and Flora, 2020), liver and kidney damage (Malin et al., 2019), mental retardation in children (Srivastava and Flora, 2020), and damage to the reproductive system and immune system (Liang et al., 2017; Shi et al., 2016; Wu et al., 2022). Among them, the impact of fluoride on the central nervous system is of particular concern due to its unique properties (low dose response, impact on neurodevelopment, and long-term effects (Pérez-Vázquez et al., 2021; Rocha-Amador et al., 2007). In particular, endemic fluorosis has been reported in many areas of China and has improved greatly in recent years (He et al., 2020; Li et al., 2023). However, in meta-analysis of people with high fluoride exposure in Canada, researchers reported that IQ, responsiveness, and abstract reasoning ability were significantly reduced in children at various levels (Goodman et al., 2022; Till et al., 2020). Neurotoxicity and memory impairment have been reported in both adults and children with prolonged ingestion of fluoride through drinking water (Choi et al., 2012; Grandjean, 2019), mainly due to the disruption of structural and functional integrity of the nervous system (Kupnicka et al., 2020). Current researches focused on the following aspects of fluoride-induced abnormalities: (1) changes in cell

* Corresponding author at: College of Life Science, Northwest Normal University, Lanzhou 730070, China.
** Corresponding author at: Department of General Surgery, Gansu Provincial Hospital, Lanzhou 730000, China.
E-mail addresses: xzhuaf@nwnu.edu.cn (X. Zhu), sallyzhangmin@126.com (M. Zhang).

https://doi.org/10.1016/j.ecoenv.2023.115752
Received 16 April 2022; Received in revised form 19 November 2023; Accepted 25 November 2023
Available online 30 November 2023

morphology and abnormal expression of cytoskeletal proteins, such as swelling of mitochondria, reduction of Nissl substance and expansion of ER (endoplasmic reticulum) (Liu et al., 2011; Chen et al., 2023), disappearance of axon spines and normal features, synapses, and mitochondrial agglutination and vacuole formation (Chen et al., 2017a); (2) oxidative stress caused a collapse of enzyme activity in the cerebrum and striatum, such as acetylcholinesterase (AChE), superoxide dismutase (SOD), catalase (CAT), and glutathione peroxidase (GPx), and promoted the apoptotic cell death process (Nkpaa and Onyeso, 2018); (3) inhibited a variety of enzyme activities related to metabolic processes such as TCA cycle enzymes, fatty acid oxidation, protein and nucleotide metabolic enzymes, oxidoreductases, and transferases(Araujo et al., 2019); (4) mainly altered the inflammatory status of the brain by aggravating pro-inflammatory cytokines such as Tumor necrosis factor-alpha (TNF-α), interleukin (IL)1β, and interleukin (IL)-6 and inhibiting the activity of the Wnt signaling pathway (Chen et al., 2017b; Zhang et al., 2022), which are involved in the etiopathogenesis of neurodegenerative diseases.

Although researches have shown that excessive fluoride administration induces oxidative stress, inflammation, and dysfunction in the brains of mice, the full description of the metabolic mechanisms has yet to be elucidated. Taking advantages of omics approaches, we could effectively collect comparative information on metabolites and related metabolic pathways in a systematic perspective. Therefore, to better define the role fluoride plays in fetal neurodevelopment, transcriptomics and metabolomics approaches were used to explain the trend of gene expression and the perturbation of metabolism in the mice brain upon fluoride uptake from maternal generation to maturity. Thus, we could draw a fine-grained spectrum of the molecular mechanism of fluoride-induced changes in the nervous system and analyze it from a global perspective to provide a basis for the dose and safety of subsequent fluoride intake.

2. Materials and methods

2.1. Animal experiments

All procedures followed the Guide for the Care and Use of Laboratory Animals: Eighth Edition (ISBN-10: 0-309-15396-4), and the animal experiment protocol was approved by the Human and Animal Experimentation Ethics Committee of Northwest Normal University and conformed to the guidelines for the care and use of animals in current Chinese legislation. Five-week-old male and female C57BL/6 J mice (n = 18 for each sex) were purchased from the Animal Center of Lanzhou University Medical Department (Lanzhou, China). The mice were housed at a temperature of 22–25 ℃ and humidity of 60 % on a 12-h light-dark cycle with free access to food and water for seven days before experimental use. Mice were divided into three groups of 12 animals each, consisting of 6 females and 6 males in different cages. The control group was treated with distilled water, and the other two groups were treated with 10 and 50 mg/L NaF (Sigma-Aldrich) in drinking water, respectively. Fluoride concentrations are considered according to the fluoride consumption adapted to the rodent metabolism in artificially fluoridated water and in fluorosis endemic areas (Dunipace et al., 1995; Eldridge et al., 2011). All animals were fed commercial rodent pellets ad libitum throughout the experiment. After 30 days, the female adult mice in the different groups became pregnant by mating with the corresponding groups of male mice. Confirmation of pregnancy was determined by identification with a vaginal tampon. The mouse offspring were continuously treated with different fluoride concentrations in the drinking water during pregnancy and lactation, which were similar to those of their parents. After postnatal day 30, 12 offspring from each group were used for further analysis. The brains were dissected immediately after treatment, frozen in liquid nitrogen, and stored at −80 ℃ until further use.

2.2. Transcriptome sequencing

Total RNA was extracted from each sample using TRIzol reagent (Life technologies, USA) according to the protocol indicated by manufacture. A total of 18 cDNA libraries were prepared from parental brain tissues of the control group (Ctl_P1), 10 mg/L NaF (T1_P1) and 50 mg/L NaF (T2_P1), and from brain tissues of the offspring of the control group (Ctl_P2), 10 mg/L NaF (T1_P2) and 50 mg/L NaF (T2_P2). Total RNA was extracted and qualified with oligo (dT) magnetic beads before mRNA enrichment. The enriched mRNA was randomly fragmented into short fragments by addition of fragmentation buffer. Using these mRNA fragments as templates and random hexamers as primers to synthesize single-stranded cDNA, the mixture of buffer, dNTPs, RNaseH and DNA polymerase I was then added to synthesize double-stranded cDNA. Then, the cDNA was purified with AMPureXP beads and the cohesive ends were modified to blunt ends with T4 and Klenow DNA polymerases. Adenine residues and DNA adaptors were then added to the 3′ ends of the fragments and AMPureXP beads were used to purify these fragments. After PCR amplification of the library, Illumina NovaseqTM 6000 was used to generate 2 × 150 bp paired end (PE) reads.

2.3. Analysis of transcriptome data

Prior to assembly, raw data were filtered by excising adaptors and low-quality reads to generate clean reads. StringTie software was used to assemble the clean reads for de novo transcriptome assembly with the reference mouse genome. The quality of the assembly was assessed by LC Bio (Hangzhou, China). Gene expression values were normalized by fragments per kilobase per million fragments (FPKM) (Li et al., 2014). Differentially expressed genes (DEGs) were selected using DESeq2 software. Compared to the corresponding control groups, genes with a $|\log2$ fold change (FC)$| > 1$ and adj p-values of less than 0.05 were considered statistically significant. Clustering heatmap was based on "ggplots2" and "Pheatmap" (Guo et al., 2021). The Gene Set Enrichment Analysis (GSEA) tool (Subramanian et al., 2005) was used to find enriched biological processes and pathways according to the product manual and using the default parameters. These pathways were then visualized using the Cytoscape (3.4.0) plug-in EnrichmentMap.

2.4. Metabolome analysis

Samples from all groups were collected in the same manner as for the RNA-seq procedure. 1 g of tissue was homogenized in liquid nitrogen and total metabolites were extracted with 400 μL methanol-acetonitrile-water solution (v: v- v = 2:2:1) by sonication for 10 × 3 min in an ice bath, then left for 10 min at −20 °C and centrifuged (14,000 g, 20 min, 4 ℃) to extract the supernatant. The supernatant was dried in the freezer and stored at −80 ℃ for LC-MS analysis. Samples were analyzed on the Thermo Scientific™ Vanquish™ UHPLC system (Thermo) as previously described. An AC18 column (Thermo Hypersil Gold C18, 100 mm × 2.1 mm, 1.8 μm) coupled to a Q Exactive mass spectrometer (Thermo) was used for detection of metabolites. The mobile phase consisted of 0.1 % formic acid in water (A) for positive mode, 5 mM ammonium acetate in water (A) for negative mode and acetonitrile (B) using the following gradient conditions: 0–1 min, 1 %B; 1–8 min, 1∼99 %B; 8–10 min, 99 % B; 10–10.1 min, 99∼1 %B; 10.1–12 min, 1 %B. The flow rate was 0.3 mL/min, the column temperature was set at 35 ℃ and the sample injection volume was 4 μL. Mass spectrometric analysis was performed with Q-Exactive mass spectrometer (Thermo Fisher Scientific, Bremen, Germany) using an electrospray ionization source in positive and negative ionization modes. The operating parameters were set as follows: Positive polarity; spray voltage 4.0 kV(positive) or −3.6 kV (negative), funnel RF lens value at 50, capillary temperature of 400 ℃, Flow rates for sheath gas, auxiliary gas and sweep gas were set to 45, 15 and 0, respectively. Unless otherwise specified, data-dependent acquisition (DDA) was used with the full MS -ddMS2 setup. The full MS

resolution was set to 70,000, and the mass range was set to 100–1500. For MS2 spectra, the resolution was set to 17, 500. Normalized collision energy was set to 20 %, 40 %, 60 %. Dynamic exclusion values were set to 5 s

2.5. Analysis of metabolome data

XCMS software (Progenesis QI, MarkerView) was used for peak alignment, retention time correction and peak area extraction. The identification of metabolites was achieved using the data extracted by XCMS. The type of adducts was selected, [M+H]+ and [M+Na]+ in positive mode and [M-H]- and [M + FA -H]- in negative mode, and the mass error value was 20 PPM. Then, each group was analyzed with orthogonal projections on latent structures, discriminant analysis (OPLS-DA), and volcano plot were used to further analyze the standardized data in the MetaboAnalyst 5.0 Online Server (http://www.metaboanalyst.ca). Finally, the differential metabolites were determined based on the variable importance in the projection value (VIP > 1) and Student's t test ($p < 0.05$) when comparing two groups. Data analysis included statistical variant analysis, multidimensional statistical analysis, differential metabolite screening and differential metabolite correlation analysis, KEGG pathway analysis were achieved using MetaboAnalyst 5.0 software.

2.6. Real-time PCR analysis

Total RNA of mouse brain samples was isolated using Trizol reagent according to the manufacturer's instructions. After measuring the RNA concentration, the RNA was transcribed into cDNA using the FastKing gDNA Dispelling RT SuperMix kit according to the manufacturer's instructions (TAKARA BIO INC, Japan) (RT). Real-time PCR (RT-PCR) was analyzed using a SYBR Green QuantiTect RT-PCR kit. PCR amplification was performed with 40 cycles: Denaturation at 95 ℃ for 10 s, annealing at 55 ℃ for 20 s, and extension at 72 ℃ for 30 s. The relative values of gene expression of each mRNA were calculated by normalization to β-actin mRNA expression using the $2^{-\triangle\triangle CT}$ method and expressed as fold values of the control. Details of primers used for RT-PCR are given in Table 1.

Table 1
The primers of real time quantitative PCR.

Gene name	Primer	Sequence
Git1	forward	CTAAAGACAGAGCAGGTCACCAA
	reverse	GCCATCTCAGTCACAGCCAAAT
P2rx6	forward	CGTGGCTGACTTTGTGAAGC
	reverse	CTGGACATCTGCCCTGGACT
Prkn	forward	CAAACAAGCAACCCTCACCTT
	reverse	CTGGCACTCACCACTCATCC
Synpo	forward	CCACCTATGCGGAGACTTTG
	reverse	AGGGGCTACCTGACCTTTCA
Stxbp1	forward	CGAGCAGCCAAAGTCATCAA
	reverse	AGCGGAGTCCAGGGAATACA
Irf7	forward	TCCAAACCCCAAGCCCTCT
	reverse	CCAGACTCGGATTCCAGTATGTG
Irf9	forward	AGCAGGAACCCTCCCTAACC
	reverse	TGCCACCACCGCCTATGTT
Alox12b	forward	CGGTACAACGTCCAGATCAATAG
	reverse	ACCATCACCTGTGCGAAGC
Cyp2u1	forward	ACCATTCCCAAAGGCACAGT
	reverse	CCGCTTCCCTATCCCAAAA
Ephx2	forward	ACGCCGTTTATGCCACCA
	reverse	GTCCGACTCATGTTCTTCTCCA
Ptges	forward	GATGAGGCTGCGGAAGAAG
	reverse	GCCGAGGAAGAGGAAAGGAT
Ptgs1	forward	TGGCTCTGGGAATTTGTGAA
	reverse	GGCTGGGGATAAGGTTGGAC

Note: *Git1,* ARF GTPase-activating protein GIT1; *P2rx6,* P2X purinoceptor 6; *Prkn,* E3 ubiquitin-protein ligase parkin; *Synpo,* Synaptopodin; *Stxbp1,* Syntaxin-binding protein 1; *Irf7,* Interferon regulatory factor 7; *Irf9,* Interferon regulatory factor 9; *Alox12b,*Arachidonate 12-lipoxygenase, 12R-type; *Cyp2u1,* Cytochrome P450 2U1; *Ephx2,* Bifunctional epoxide hydrolase 2; *Ptges,* Prostaglandin E synthase; *Ptgs1,* Prostaglandin G/H synthase 1.

2.7. Statistical analysis

IBM SPSS Statistics 25 for Windows was used for data analysis. Data with normal distribution were presented as means ± standard deviation (SD), and the t-test for independent samples was used to analyze differences between two groups. Gene expression differences were considered statistically significant when the $p < 0.05$. For metabolome profiling, all the original data sets were uploaded into MetaboAnalyst 5.0 and performed principle component analysis(PCA) and partial least-squares discriminat analysis (PLS-DA). Variable importance in projection (VIP) score and ANOVA were used to evaluate the significant accumulated metabolites between groups with the threshold greater than 1, and $p < 0.05$ were considered significant.

3. Results

3.1. Effects of fluoride on global transcriptome pattern in mouse brain

To investigate the molecular signature of fluoride induced brain damage, the disturbed gene expression patterns after fluoride administration were characterized by transcriptome profiling. The brain tissues of parental control group (Crtl_P1), 10 mg NaF treatment (T1_P1), 50 mg NaF treatment (T2_P1) and offspring control group (Crtl_P2), 10 mg NaF treatment (T1_P2), 50 mg NaF treatment (T2_P2) were collected. Total RNA from 6 different sample groups was extracted and 18 libraries were prepared to perform RNA-seq analysis. The Q30 in each sample was above 96.8 %. Of the clean reads, over 95.85 % in each sample were successfully aligned to the reference genome. The annotation information of the unigenes were obtained from the Swiss-Prot and pfam databases.

Differential expression of genes was calculated using DEseq2 algorithm in different groups based on FPKM values, comparing log2 (fold change) >1 (up-regulated) or <1 (down-regulated) and *p*-value <0.05 simultaneously. There were 238 genes significantly up-regulated between Crtl_P1 and T1_P1 groups, while 66 genes were significantly down-regulated, and for the high-dose parent groups, 179 (up) and 126 (down) genes showed significant changes; for offspring groups, 61 (up) and 299 (down) genes were identified between Crtl_P2_vs_T1_P2, and 152 (up) and 275 (down) genes were identified between Crtl_P2_vs_T2_P2, as shown in the column figure (Fig. 1A and 1B). The global changes in gene expression between the different groups were shown in heat maps (Fig. 1C and 1D) and in Supplemental Table 1. Representative differential gene expressions were validated by RT-PCR (see Fig. 1E and 1F).

To gain insight into the most enriched pathways of gene expression patterns during fluoride exposure, we performed a Gene Set Enrichment Analysis (GSEA) using the Read Count data matrix. The most regulated gene sets in the comparison between T1_P1 and Ctrl_P1 were mainly enriched in the decrease of neuronal synaptic functions (Fig. 2A and 2B). When comparing the parental high dose group with the control group (T2_P1 versus Ctrl_P1), neurodevelopment and synaptic functions were down-regulated similarly to the low dose group;while the immune process and neuroinflammatory responses were significantly activated (Fig. 2C and 2D).

In contrast, the offspring with low fluoride intake (T1_P2 versus Ctrl_P2) did not show a similar pattern compare to their parental groups. The up-regulated gene sets were mainly enriched in cytokine-mediated immune response, antigen display and neuronal apoptosis (Fig. 3A and 3B). At the same time, the high-dose offspring group (T2_P2 versus Ctrl_P2) showed a dramatic increase in synaptic ion transport (Fig. 3C and 3D).

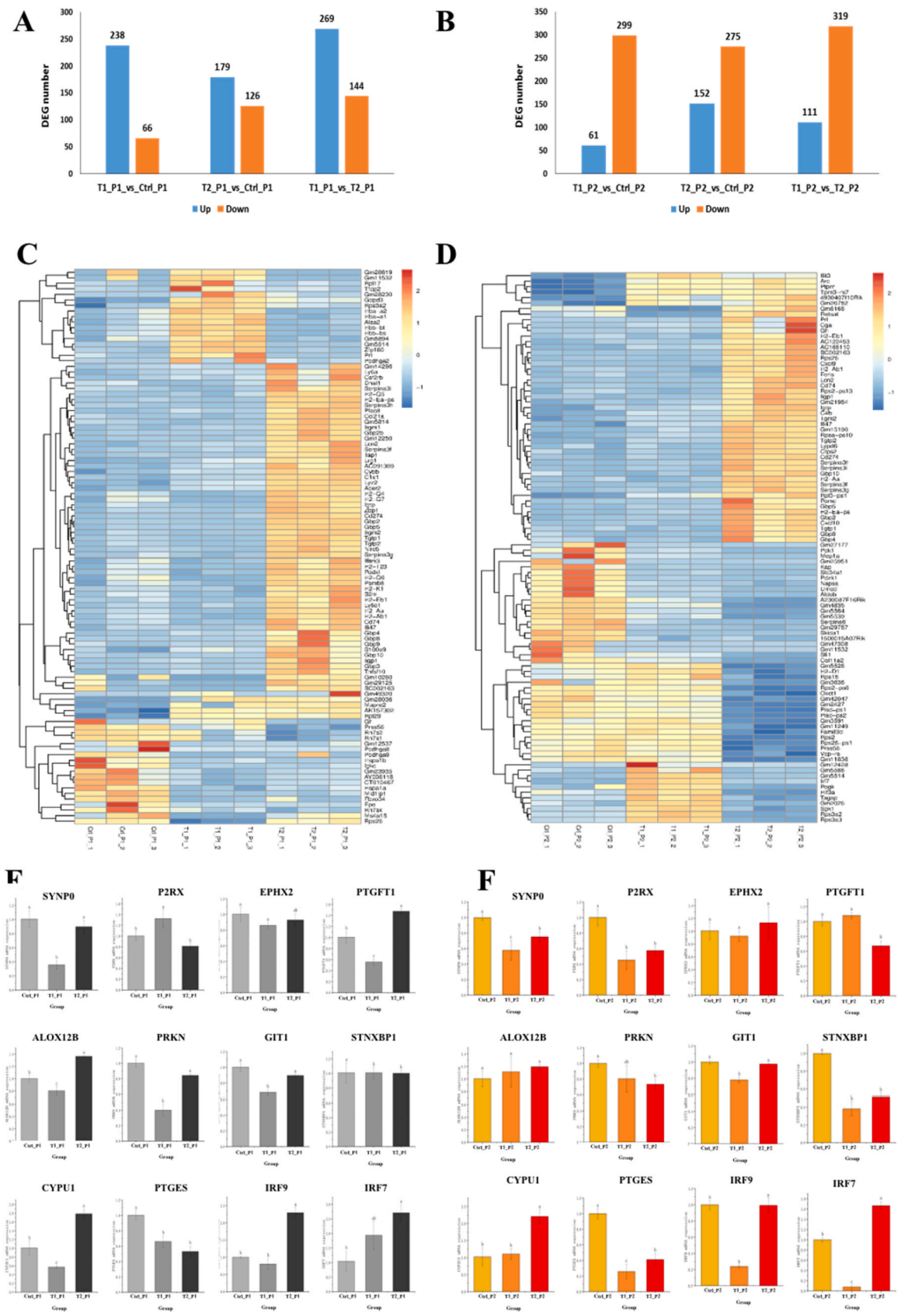

Fig. 1. Analysis of genes with differential expression. Number of genes with differential expression between different parental groups (A) and offspring groups (B); cluster analysis of differentially expressed genes on the heat map of parental groups (C) and offspring groups (D) (log2 (fold change) > 1 (up-regulated) or < 1 (down-regulated) and p-value < 0.05). Comparison of relative expression levels between different parental groups (E) and offspring groups (F) using RT-PCR verification.

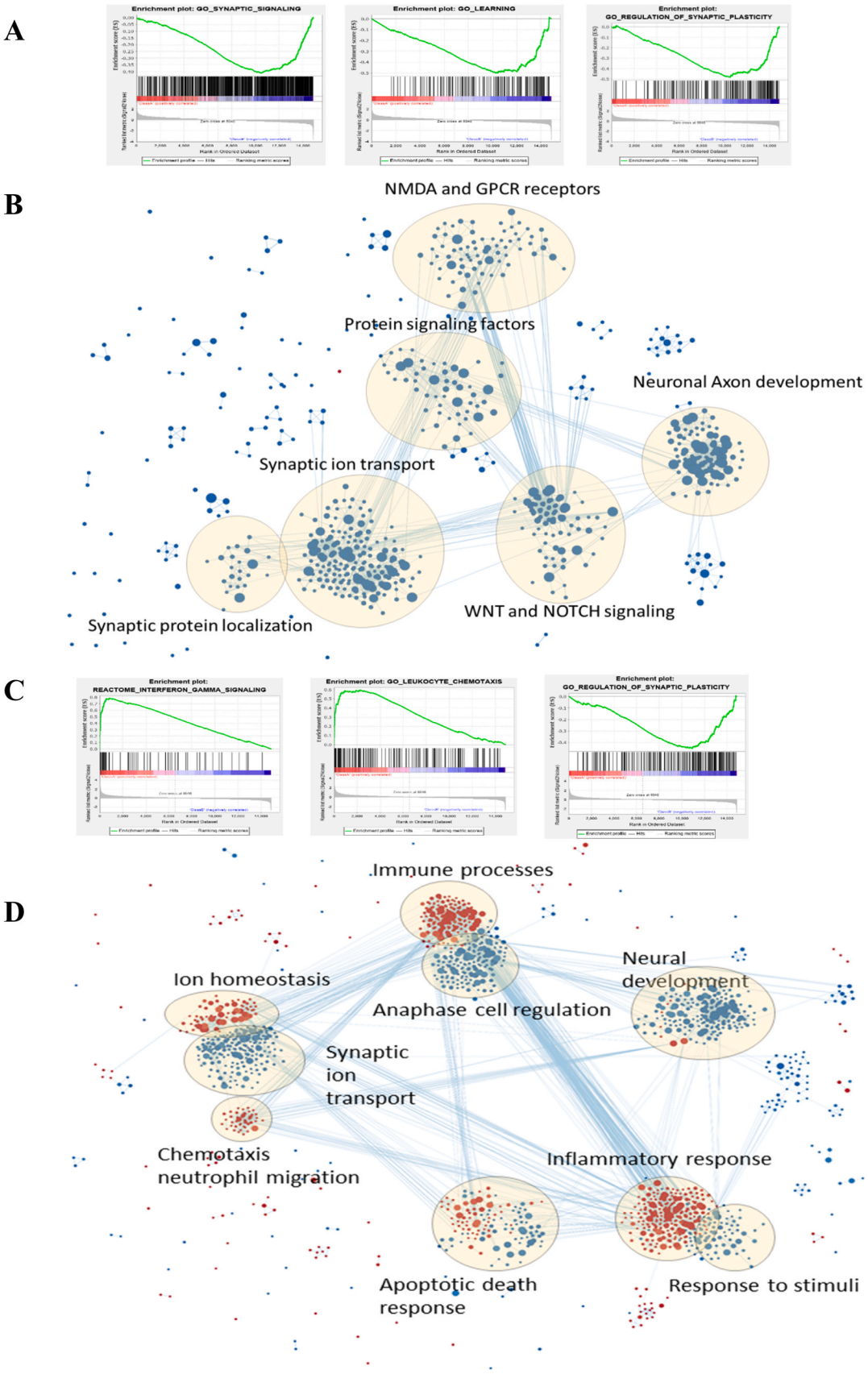

Fig. 2. Parental mice brain undergo transcriptomic changes toward decreased neuronal functions and increased inflammatory responses. (A) Gene Set Enrichment Analysis (GSEA) of top 3 regulated pathways and (B) Enrichment map of gene sets in the comparison between T1_P1 and Ctrl_P1 or (C and D) T2_P1 and Ctrl_P1(GSEA*p* value < 0.01, EnrichmentMap FDR < 0.05).

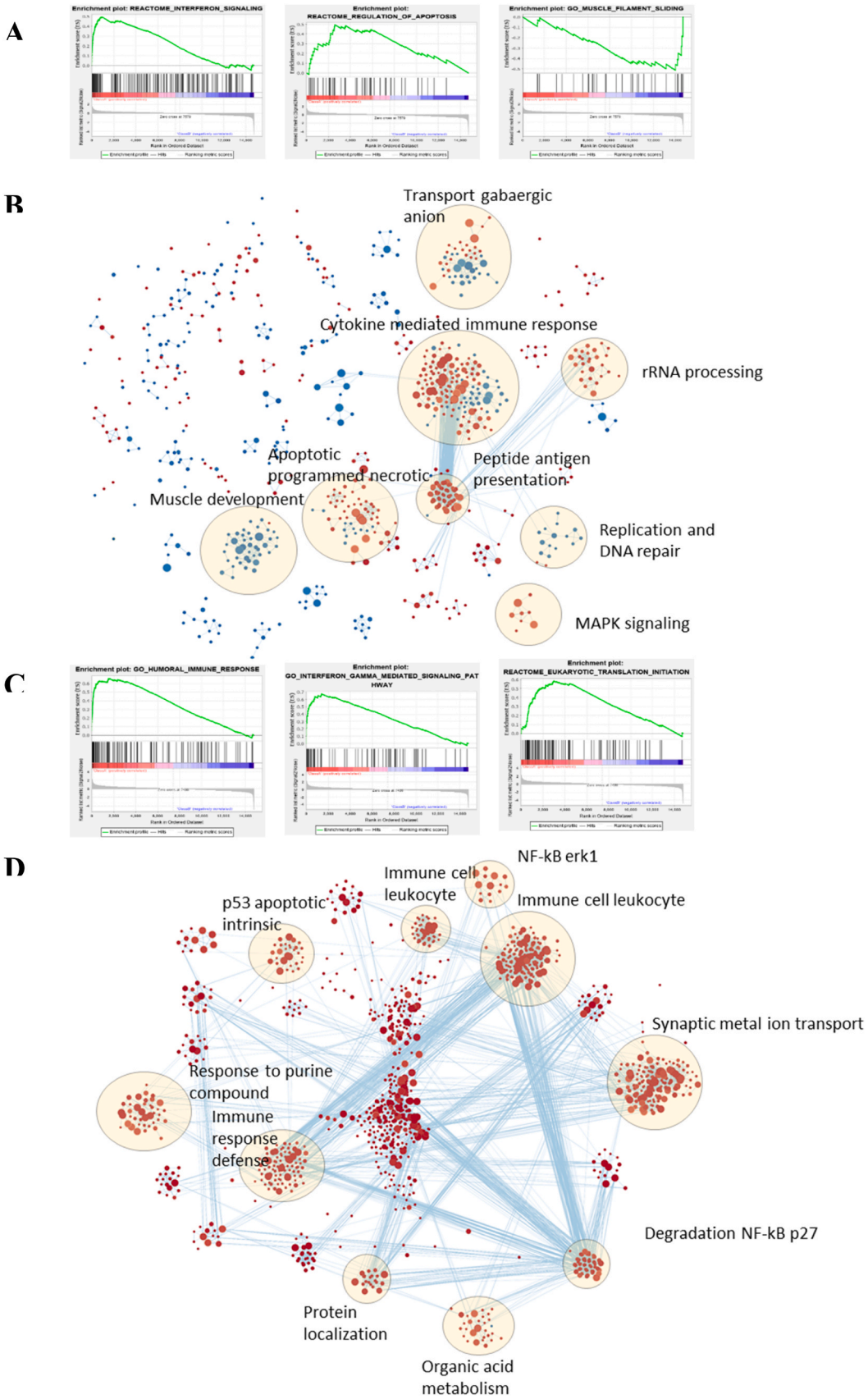

Fig. 3. Offspring mice brain undergo transcriptomic changes toward increased multiple pathways including immune response and synaptic ion transport. (A) Gene Set Enrichment Analysis (GSEA) of top 3 regulated pathways and (B) Enrichment map of gene sets in the comparison between T1_P2 and Ctrl_P2 or (C and D) T2_P2 and Ctrl_P2(GSEA p value < 0.01, EnrichmentMap FDR < 0.05).

3.2. Effects of fluoride on global metabolome pattern in mice brain

To further identify the differential accumulated metabolites responsible for the impairment of neuronal function during fluoride administration, both parental and offspring brain tissues were subjected to metabolome profiling by LC-MS /MS based untargeted metabolomics approach. The identified metabolites and intensity of correspondence were used to analyze the correlation between samples. Principal component analysis (PCA) and partial least squares discriminant analysis (PLS-DA) showed clear separation of the different sample groups. The metabolome profiling data could be considered reliable (Fig. 4A). All differentially accumulated metabolites were filtered out based on criteria such as variable importance in projection (VIP) > 1, log2 (fold change) > 1 (up-regulated) or < 1 (down-regulated) and *p*-value < 0.05 between different groups.

The identified differentially accumulated metabolites (DAMs) contain various organic compounds such as amino acids, lipids, carbohydrates, and nucleic acids. The distribution of significantly up- and down-regulated metabolites in the different groups are shown in supplemental Table 2 and Fig. 4B, 4D. Pathway enrichment analysis indicated that in parental low dose group (T1_P1 versus Ctrl_P1), nicotine addiction, synaptic vesicle cycle, cholinergic synapse were down-regulated, while mineral absorption, central carbon metabolism in cancer and protein digestion and absorption were up-regulated. In

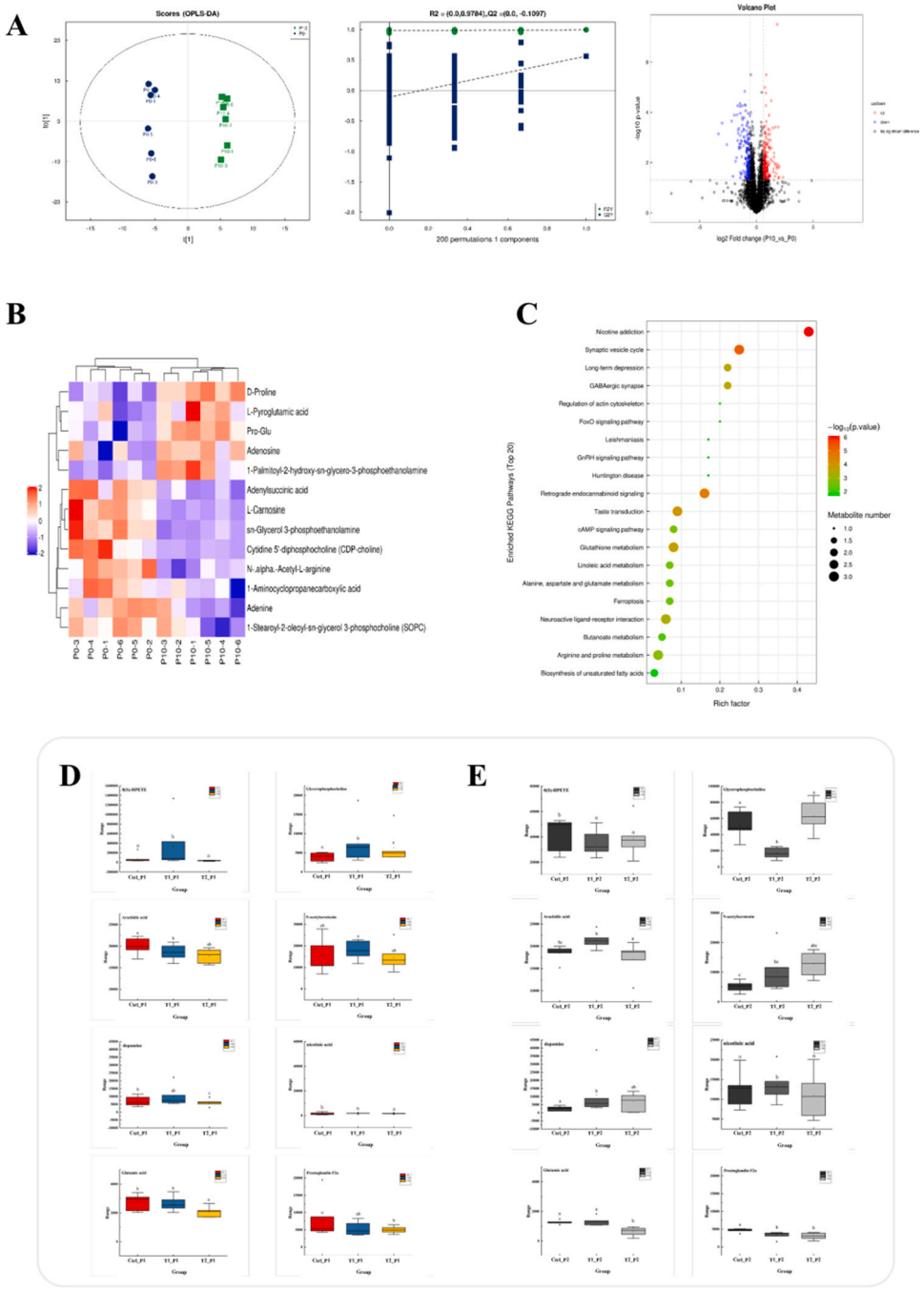

Fig. 4. The effect of fluoride exposure on global metabolomics profiles in the mice brain. (A) OPLS-DA -scores plot (left), replacement test (middle) and volcano plot (right) of parental control group and low-dose group; (B) heatmap and (C) pathway analysis of different metabolites (T1_P2 and Ctrl_P2 comparison for illustration only, other comparisons can be found in the supplemental files), representative metabolites for parental groups (D) and offspring groups (E).

parental high dose group (T2_P1 versus Ctrl_P1), metabolites closely related to glycerophospholipids metabolism and linoleic acid metabolic pathway were significantly up-regulated, and choline metabolism were significantly down-regulated. This part of results have agreed well with transcriptome data in which synaptic function were greatly inhibited.

When comparing T1_P2 and Ctrl_P2 groups, up-regulated metabolites were mainly enriched in fatty acid metabolism, and glutathione metabolism, While glycerophospholipid metabolism and taste transduction were down-regulated. At the same time, In the high dose offspring group (T2_P2 compared with Ctrl_P2), synaptic vesicle cycle, GABAergic synapse and neuroactive ligand-receptor interaction were up-regulated, while pyrimidine metabolism and alpha-linolenic acid metabolism were down regulated. These results were also corresponding with the transcriptome data where T2P2 group showed the trend of synaptic metal ion transport elevation (Fig. 3).

3.3. Combined enrichment analysis of transcriptome and metabolome

To further investigate the relationship between fluoride induced developmental neurotoxicity and metabolism pathways, we performed a combined metabolome and transcriptome analysis to screen out the core metabolism pathways. We found that the expression of choline-related metabolites, catalytic enzymes, metabolic derivatives, and their receptors was dose-dependent and differed between generations by comparing the co-regulated metabolic pathways (Fig. 5). The accumulation of cytidine 5′-diphosphocholine (CDP-choline), phosphatidylcholine (Ptd-choline), and lysophosphatidyl choline (lyso-Ptd-choline) in parental groups were significantly up-regulated, whereas the accumulation of CDP-choline in offspring brains showed a downward trend. The accumulation of acetylcholine was significantly decreased while glyceraldehyde-3-phosphate (G3P) and choline were not changed in the parental groups, whereas upward trends of those metabolites were observed in the offspring. In addition, we found that arachidonic acid and its metabolic precursors (such as phosphotidylethandamine, linoleate, arachidonate) tended to show an opposite accumulation trend between high-dose and low-dose groups in offspring mice brain. Arachidonic acid-derived prostaglandins can act as proinflammatory mediators between cells, contributing to the development of inflammation and promoting the aggravation of pain (Jang et al., 2020). The expression of prostaglandin receptors showed a consistent trend toward up-regulation in both generations. At the same time, the regulation of glutamate, adenosine, and acetylcholine was different in the high and low dose groups, whereas the expression of downstream regulatory genes such as cAMP response element binding protein (CREB) and c-FOS showed a consistent downward trend (Fig. 5) majorly in parental mice brain.

4. Discussion

Numerous studies have demonstrated the developmental neurotoxicity of fluoride, especially during the perinatal period, when fluoride can enter the brain of the offspring through the placental barrier and the blood-brain barrier, thereby causing irreversible damage to the developing nervous system. (Goodman et al., 2022; Pérez-Vázquez et al., 2021; Rocha-Amador et al., 2022; Till et al., 2020). Brain mophology change and neuronal cell damage induced by fluoride mainly caused by activation of ROS, neuroinflammation, and apoptosis (Ge et al., 2018). The presynaptic and postsynaptic membrane could be affected by fluoride in a hairy manner, and postsynaptic density thickens and vacuolization of mitochondria was also observed (Niu et al., 2018). Fluoride can reduce glutamate levels in the cerebral cortex and hippocampus of mice (Ottappilakkil et al., 2023). In addition, the activity of enzymes related to glutamate metabolism in the hippocampus, including glutamate decarboxylase (GAD), glutamate oxaloacetic acid (GOT) and glutamate acetone aminotransferase (GPT) (Bartos et al., 2019), are also affected, leading to learning and memory impairment (Agalakova and Nadei, 2020). During the development of the nervous system, fluoride can affect dopamine concentrations and dopamine receptors (D1R and D2R) in the striatum and cerebellum and impair the function of dopaminergic pathways (Kupnicka et al., 2020). However, the relationship between synaptic function and metabolite accumulation espacilly for developmental neurotoxicity, are not yet clear. Here, we integrated the transcriptome and metabolome to comprehensively investigate the core metabolism pathways between parents and offspring upon fluoride administration.

As shown in Figs. 2 and 3, synaptic vulnerability and neurotransmitter dysfunction correlated in a dose- and generation-dependent manner, while neurotransmitters such as acetylcholine and L-glutmate were less accumulated in T1_P1 compared to Ctrl_P1 in metabolomics profiling (Figs. 4B and 4 C). Genes involved in synaptic functions, such as ARF GTPase-activating protein (*GIT1*), Purinergic Receptor P2×6 (*P2RX6*), Parkin RBR E3 Ubiquitin Protein Ligase (*PRKN*), Synaptopodin

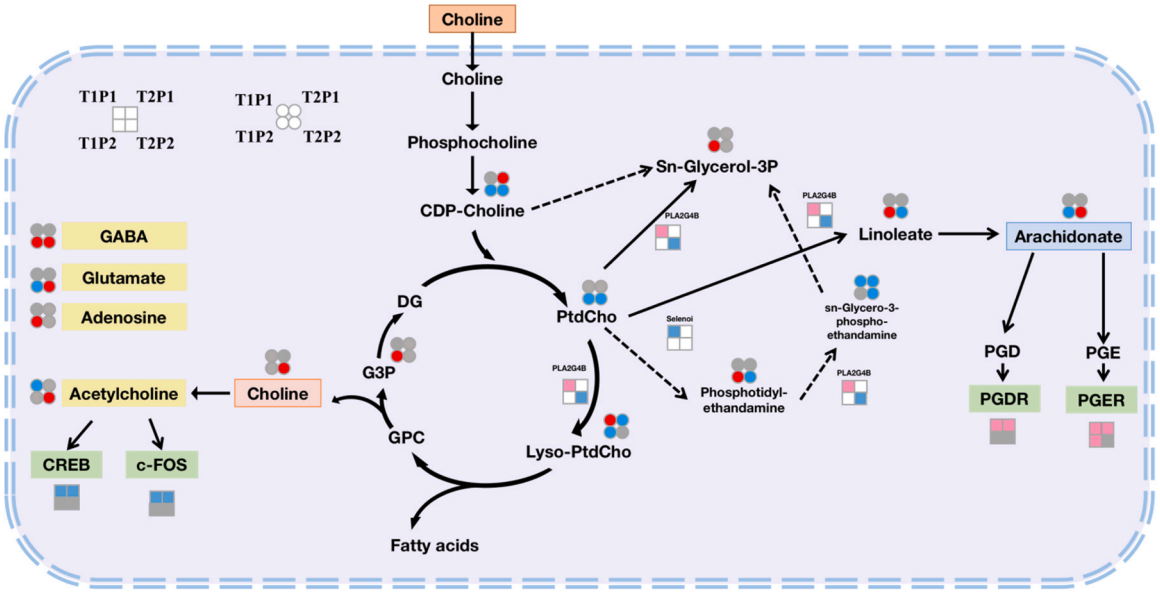

Fig. 5. Integrative analysis of metabolism pathways during fluoride exposure. Circular means metabolites, square means metabolism enzymes. Statistically significant changes in metabolites and gene expression are shown as red (up-regulated) or blue (down-regulated).

(*SYNPO*), Syntaxin-binding protein 1 (*STXBP1*), etc., were also affected and confirmed by RT -Q-PCR (Figs. 1E and 1 F). STXBP1 protein is part of the Soluble NSF attachment protein receptors (SNARE) complex and plays an important role in the release of synaptic vesicles, especially neurotransmitters in the synapse. The link between STXBP1 and acetylcholine has been revealed in *c-elegans* studies and shown that STXBP1 could affect acetylcholine release (Rezazadeh et al., 2019). The GIT1 protein also plays an important role in regulating the endocytic trafficking of G protein-coupled receptors, including dopamine receptors (Kim et al., 2017). In current study, both in parental and offspring mice brain, fluoride administration could effectively decrease the expression of STXBP1 and GIT gene, and showed a positve correlation with the accumulation of acetylcholine. For glycerophosphocholine, one of the precursors of the neurotransmitter acetylcholine, can be converted to phosphorylcholine, which is an active form of choline that reaches cholinergic synaptic terminals and increases acetylcholine synthesis and release. In addition, glycerophosphocholine could positively affect the expression of choline uptake transporters (*CHT*) and vesicular acetylcholine transporters (*VAChT*), resulting in improved synaptic efficiency (Tomassoni et al., 2012; Semproli et al., 2021). Therefore, low-dose fluoride administration in the parental group could effectively reduce the accumulation of neurotransmitters and related metabolites while inhibit synaptic function and synaptic ion transport (Fig. 2).

In the integrative analysis of transcriptomic and metabolomics, we found that the most significant changes between the parental and offspring were in the choline recycling metabolic pathway and arachidonic acid metabolism. Most interestingly, the accumulation of acetylcholine and the expression of synaptic transport-related genes were down-regulated in the parental group and up-regulated in the offspring group, which shown a reversed trend; while glutamate and arachidonic acid were down-regulated in low-dose offspring group and up-regulated in high-dose offspring group. This phenomenon has never been reported in previous studies. Based on the progress of existing studies and the results of present study, the explanation for this phenomenon seems to have two possibilities at present:

(1) The offspring mice were continuously exposed to excessive fluoride during pregnancy and lactation, and the overall process of brain neuronal development could be significantly different from that of the non-intake group. From the transcriptomic and metabolomic results, the offspring mice in the high-dose group had a significant activation of inflammation-related signals compared with the control group, but at the same time their synaptic transport-related pathways and choline metabolic recycling pathways were also extensively activated. Therefore, we have reason to believe that the choline cycle and related metabolic pathways were persistently altered after the parental intake of excessive fluorine. Such alterations may also be responsible for the abnormalities in inflammatory responses and neurodevelopmental processes.
(2) The offspring mice may have developed certain stress response mechanisms after excessive fluoride intake during pregnancy and lactation in order to continue to survive in this environment. As a result, their neurotransmitter synthesis and metabolic pathways might be altered at the level of epigenetic regulation. It is possible that such alterations are a manifestation of the organism's active defense, and that the offspring, may be able to counteract the damage caused by fluoride by making synaptic transport and neurotransmitter synthesis more active. However, at the same time, the continued accumulation of fluoride causes an inflammatory response and oxidative stress that cannot be counteracted from the perspective of organismal protection.

5. Conclusion

First, fluoride exposure during pregnancy and lactation may cause neurodevelopmental disorders in the offspring mice, including abnormal expression of genes related to synaptic function, and aneurotransmitters' accumulation; the magnitude and spectrum of response to fluoride exposure in parents and offspring are significantly different.

Second, in mice exposed to fluoride during gestation and lactation, metabolic accumulation of choline and arachidonic acid and their derivatives are the most important marker related to developmental neurotoxicity. This scenario is reported here for the first time.

Our study shows the correlation and difference between two generations of gene expression and metabolite accumulation in fluoride-exposed mice during pregnancy and lactation. We also found that choline and arachidonic acid metabolism pathways played the central role in neurodevelopmental disorders caused by fluoride uptake, and that further experiments need to be conducted to explore the regulatory mechanisms.

CRediT authorship contribution statement

Xinliang Zhu and **Ming Zhang:** Supervision, Conceptualization , Writing - Reviewing and Editing; **Xiaopeng Wang** and **Xinyu Zhu:** Methodology, Software; **Shunbin Zhang** and **Xiaoxiao Liu: Software**, Validation; **Huixia Li** and **Ji Zhang:** Data curation.

Declaration of Competing Interest

The authors declare that they have no known competing financial interests or personal relationships that could have appeared to influence the work reported in this paper.

Data availability

Data will be made available on request.

Acknowledgments

This research work was supported by Project for promoting the innovative capability of college and university from Gansu Province Education Department to Xinliang Zhu (No. 2060), The Natural Science Foundation of Gansu Province in China (21JR7RA113, 21JR7RA563) to Xinliang Zhu, The Natural Science Foundation of Gansu Province in China (21JR7RA636) to Xinyu Zhu. Basic Science Fund for Creative Research Groups of Gansu Province in China (22JR5RA709) to Min Zhang.

Appendix A. Supporting information

Supplementary data associated with this article can be found in the online version at doi:10.1016/j.ecoenv.2023.115752.

References

Agalakova, N., Nadei, O., 2020. Inorganic fluoride and functions of brain. Crit. Rev. Toxicol. 50, 28–46.
Araujo, T.T., et al., 2019. Changes in energy metabolism induced by fluoride: insights from inside the mitochondria. Chemosphere 236, 124357.
Bartos, M., et al., 2019. Effects of perinatal fluoride exposure on short-and long-term memory, brain antioxidant status, and glutamate metabolism of young rat pups. Int. J. Toxicol. 38, 405–414.
Chen, L., et al., 2017a. The effects of fluoride on neuronal function occurs via cytoskeleton damage and decreased signal transmission. Chemosphere 185, 589–594.
Chen, L., et al., 2023. Fluoride exposure disrupts the cytoskeletal arrangement and ATP synthesis of HT-22 cell by activating the RhoA/ROCK signaling pathway. Ecotoxicol. Environ. Saf. 254, 114718.
Chen, R., et al., 2017b. Fluoride induces neuroinflammation and alters Wnt signaling pathway in BV2 microglial cells. Inflammation 40, 1123–1130.
Choi, A.L., et al., 2012. Developmental fluoride neurotoxicity: a systematic review and meta-analysis. Environ. Health Perspect. 120, 1362–1368.
Dunipace, A., et al., 1995. Effect of aging on animal response to chronic fluoride exposure. J. Dent. Res. 74, 358–368.

Eldridge, D.J., et al., 2011. Impacts of shrub encroachment on ecosystem structure and functioning: towards a global synthesis. Ecol. Lett. 14, 709–722.
Ge, Y., et al., 2018. Fluoride-induced alterations of synapse-related proteins in the cerebral cortex of ICR offspring mouse brain. Chemosphere 201, 874–883.
Goodman, C.V., et al., 2022. Domain-specific effects of prenatal fluoride exposure on child IQ at 4, 5, and 6–12 years in the ELEMENT cohort. Environ. Res. 211, 112993.
Grandjean, P., 2019. Developmental fluoride neurotoxicity: an updated review. Environ. Health 18, 1–17.
Guo, H., et al., 2021. Identification of stemness-related genes for cervical squamous cell carcinoma and endocervical adenocarcinoma by integrated bioinformatics analysis. Front. Cell Dev. Biol. 9, 642724.
He, X., et al., 2020. Groundwater arsenic and fluoride and associated arsenicosis and fluorosis in China: occurrence, distribution and management. Expo. Health 12, 355–368.
Jang, Y., et al., 2020. Molecular mechanisms underlying the actions of arachidonic acid-derived prostaglandins on peripheral nociception. J. Neuroinflamm. 17, 1–27.
Kim, H., et al., 2017. Interaction effects of GIT 1 and DRD 4 gene variants on continuous performance test variables in patients with ADHD. Brain Behav. 7, e00785.
Kupnicka, P., et al., 2020. Fluoride affects dopamine metabolism and causes changes in the expression of dopamine receptors (D1R and D2R) in chosen brain structures of morphine-dependent rats. Int. J. Mol. Sci. 21, 2361.
Li, B., et al., 2014. Evaluation of de novo transcriptome assemblies from RNA-Seq data. Genome Biol. 15, 1–21.
Li, F., et al., 2023. Soil exposure is the major fluoride exposure pathways for residents from the high-fluoride karst region in Southwest China. Chemosphere 310, 136831.
Liang, S., et al., 2017. Sodium fluoride exposure exerts toxic effects on porcine oocyte maturation. Sci. Rep. 7, 1–14.
Liu, Y.-J., et al., 2011. Increased level of apoptosis in rat brains and SH-SY5Y cells exposed to excessive fluoride—a mechanism connected with activating JNK phosphorylation. Toxicol. Lett. 204, 183–189.
Malin, A.J., et al., 2019. Fluoride exposure and kidney and liver function among adolescents in the United States: NHANES, 2013–2016. Environ. Int. 132, 105012.
Niu, R., et al., 2018. Effects of fluoride on synapse morphology and myelin damage in mouse hippocampus. Chemosphere 194, 628–633.
Nkpaa, K.W., Onyeso, G.I., 2018. Rutin attenuates neurobehavioral deficits, oxidative stress, neuro-inflammation and apoptosis in fluoride treated rats. Neurosci. Lett. 682, 92–99.
Ottappilakkil, H., et al., 2023. Fluoride induced neurobehavioral impairments in experimental animals: a brief review. Biol. Trace Elem. Res. 201, 1214–1236.
Pérez-Vázquez, F., et al., 2021. Health risk assessment in children living in an urban area with hydrofluorosis: San Luis Potosí Mexico case study. J. Trace Elem. Med. Biol. 68, 126863.
Rezazadeh, A., et al., 2019. STXBP1 encephalopathy is associated with awake bruxism. Epilepsy Behav. 92, 121–124.
Rocha-Amador, D., et al., 2007. Decreased intelligence in children and exposure to fluoride and arsenic in drinking water. Cad. De. saúde pública 23, S579–S587.
Rocha-Amador, D.O., et al., 2022. Health risk assessment in Mexican children exposed to fluoride from sweetened beverages. Biol. Trace Elem. Res. 1–8.
Semproli, R., et al., 2021. Chemical and enzymatic approaches to esters of sn-glycero-3–phosphoric acid. Eur. J. Org. Chem. 2021, 4027–4037.
Shi, Z., et al., 2016. Effects of fluoride on the expression of p38MAPK signaling pathway-related genes and proteins in spleen lymphocytes of mice. Biol. Trace Elem. Res. 173, 333–338.
Srivastava, S., Flora, S., 2020. Fluoride in drinking water and skeletal fluorosis: a review of the global impact. Curr. Environ. Health Rep. 7, 140–146.
Subramanian, A., et al., 2005. Gene set enrichment analysis: a knowledge-based approach for interpreting genome-wide expression profiles. Proc. Natl. Acad. Sci. 102, 15545–15550.
Till, C., et al., 2020. Fluoride exposure from infant formula and child IQ in a Canadian birth cohort. Environ. Int. 134, 105315.
Tomassoni, D., et al., 2012. Effects of cholinergic enhancing drugs on cholinergic transporters in the brain and peripheral blood lymphocytes of spontaneously hypertensive rats. Curr. Alzheimer Res. 9, 120–127.
Wu, S., et al., 2022. Challenges of fluoride pollution in environment: mechanisms and pathological significance of toxicity–a review. Environ. Pollut. 304, 119241.
Zhang, C., et al., 2022. NaF-induced neurotoxicity via activation of the IL-1β/JNK signaling pathway. Toxicology 469, 153132.